Available online at www.sciencedirect.com
SCIENCE DIRECT®
International Journal of Hydrogen Energy 31 (2006) 752–761
International Journal of HYDROGEN ENERGY
www.elsevier.com/locate/ijhydene

Experimental studies and comprehensive reactor modeling of hydrogen production by the catalytic reforming of crude ethanol in a packed bed tubular reactor over a Ni/Al_2O_3 catalyst

Ahmed Aboudheir[a], Abayomi Akande[a,b], Raphael Idem[a,*], Ajay Dalai[b]

[a] *Process Systems Engineering Laboratory, Faculty of Engineering, University of Regina, Regina, Canada S4S 0A2*
[b] *Chemical Engineering Department, University of Saskatchewan, Saskatoon, Canada S7N 5C5*

Available online 2 August 2005

Abstract

A rigorous numerical model was developed to simulate the production of hydrogen from the reforming of crude ethanol in a packed bed tubular reactor (PBTR). The model was based on the coupling of mass and energy balance equations as well as a new kinetic model developed for the process. The simulation results for crude ethanol conversion were found to be in accordance with the experimental data obtained at various operating conditions. This confirms the validity of the numerical model. A further validation of the model was obtained by using the model to simulate a well-documented reaction process. In addition, the predicted variations of the concentration and temperature profiles for our process in the radial direction indicate that the assumption of plug flow and isothermal behavior is justified within certain kinetics operating conditions. However, even within these operating conditions, our results have proven that the axial dispersion terms in both the mass and the energy balance equations cannot be neglected.

Keywords: Hydrogen; Crude ethanol; Reforming; Kinetics; Tubular reactor modeling

1. Introduction

Strong efforts are being made to commercialize the use of fuel cells such as the proton exchange membrane (PEM) fuel cell for the generation of electric power for both electric vehicles and distributed stationary applications [1,2]. The major reason for the interest is the high-energy efficiency of the fuel cell, which in some cases, is reported to have an overall energy efficiency of about 85% [3]. Also, with an equally strong interest in the use of hydrogen (H_2) as the fuel, PEM fuel cells are the most certain to meet future ultra low NO_x, SO_x, CO, CH_4 and CO_2 emissions targets [1]. Thus, H_2 has a significant future potential as an alternative fuel that can solve the problems of CO_2 emissions as well as the emissions of other air contaminants. It is well known that H_2 production can be accomplished by gasification or reforming of fossil fuels [4,5] or biomass [6]. However, if a global cycle of clean and sustainable production of energy is envisaged, a new eco-friendly reservoir of hydrogen is needed [7,8].

In this context, ethanol (a form of biomass) satisfies most of these requirements since it is easy to produce, and is also safe to handle, transport and store [9,10]. As such, ethanol provides an environmentally responsible energy source that can significantly reduce greenhouse gas emissions [8]. It is also known that the application of ethanol for the production and use of H_2 energy is CO_2 neutral [11]. Furthermore, since ethanol does not contain heteroatoms and metals, its use as source of energy does not result in emissions of NO_x, SO_x, particulates and other toxics. In addition, ethanol is mostly an oxygenated hydrocarbon, which leads to complete

* Corresponding author. Fax: +1 306 585 4855.
E-mail address: Raphael.idem@uregina.ca (R. Idem).

0360-3199/$30.00
doi:10.1016/j.ijhydene.2005.06.020

combustion during its application to produce power. As such, little or no CO is produced. These attributes have made H_2 obtained from ethanol reforming a very good energy vector, especially in fuel cells applications. H_2 production from ethanol has advantages when compared with other H_2 production strategies, including steam reforming of methanol and hydrocarbons. Unlike hydrocarbons, ethanol is easier to reform and is also free of sulfur, which is a catalyst poison in the reforming of hydrocarbons [9]. Also, unlike methanol, which is sourced from hydrocarbons [12] and has a relatively high toxicity, ethanol is completely biomass based and has low toxicity.

The production of hydrogen by steam reforming of pure ethanol has been widely investigated [13–16]. In all these cases, water is needed as a co-feed to the process. Consequently, there is no need to reduce the water and organic contents of wet or crude ethanol (i.e. fermentation broth produced from a fermentation process) since this contains approximately 12% v/v ethanol, which is within the range of water to ethanol molar ratios used for the literature cited ethanol reforming processes. Besides, by using crude ethanol, the other organic compounds present in the fermentation broth could equally be reformed to produce additional H_2. Also, this process would eliminate the large amount of energy wasted during distillation to remove water from fermentation broth in order to produce dry or pure ethanol. Haga et al. [8] suggested that in order to obtain a widespread use of ethanol for hydrogen production, the economics and energetics of the ethanol production process have to be greatly improved. Thus, by circumventing the distillation and drying step, our process [17,18] of reforming crude ethanol (i.e. fermentation broth) provides us with the ability to produce H_2 from crude ethanol solution in a cost-effective manner. We recently developed the catalytic process for H_2 production from the reforming of crude ethanol based on $Cu/Mn/Al_2O_3$ and Ni/Al_2O_3 catalysts [17–19].

Because of weight and engineering problems, on-board reforming to produce H_2 no longer appears to be the most attractive way to deliver H_2 to the fuel cell in electric vehicles. Instead, there are strong efforts to deliver the H_2 to the fuel cell for this application by means of H_2 refueling stations. Several such stations already exist, for example, the Hydrogenics station in Toronto, Canada, as well as the ones in Perth, Australia and in Japan. A very important aspect for the actualization of the PEM fuel cell powered electric vehicles and distributed stationary PEM energy application (especially in remote locations where biomass is abundant) that would use crude ethanol based H_2 is the proper design of the crude ethanol reformer. It is well known that the simulation and design of any reactor requires information on both the thermodynamic and kinetic properties of the reaction of interest. In this regard, we have recently developed the kinetics for the production of hydrogen by the reforming of crude ethanol in a packed bed tubular reactor (PBTR) over 15% Ni/Al_2O_3 catalyst prepared by coprecipitation techniques [19].

It is well known that catalytic PBTRs are usually used for the reforming of hydrocarbons [20] or the reforming of oxygenated hydrocarbons such as methanol and ethanol. The performance of these reactors (tubular and membrane) depends on the mass transport characteristics and temperature distribution in the reactor. Most of the reported design models in the literature are based on unrealistic assumptions such as plug flow behavior, perfectly isothermal or adiabatic condition, or negligible radial gradients [21–23], which were imposed mainly to obtain a simple model to solve in terms of ordinary differential equations. However, this simplification may be a serious deficiency when reactions with pronounced heat effects are involved such as in the hydrocarbon or oxygenated hydrocarbon reformation processes. Only few recent papers exist in the literature, which have reported models that take into consideration the variations of the concentration and temperature in both the axial and radial directions. However, these models still apply several assumptions such as negligible pressure drop, ideal behavior of gases, constant reactor wall temperature, negligible diffusion resistance of particle of catalyst, or negligible axial dispersion [24,25]. It is well known that the more unrealistic the assumptions imposed on the model are, the less accurate will the model be able to predict the behavior of the process. In this paper a comprehensive numerical model was solved and compared with experimental results in order to investigate the validity of some of these assumptions for the production of hydrogen from the reforming of crude ethanol in a PBTR.

2. Theory

2.1. Numerical modeling

The numerical model developed and used for modeling and simulation of the PBTR is based on the steady state mass and energy balances (Eqs. (1) and (2), respectively) around the reactor in the presence of chemical reactions. Based on the general mass and energy balance equations reported by Bird et al. [26] and the geometry of the PBTR depicted in Fig. 1, which represents a schematic diagram of the catalytic PBTR used in the experimental work, the model equations can be presented in cylindrical coordinates for z components as in Eqs. (1) and (2):

$$v_Z \frac{\partial C_i}{\partial z} = D_r \left(\frac{\partial^2 C_i}{\partial r^2} + \frac{1}{r} \frac{\partial C_i}{\partial r} \right) + D_z \frac{\partial^2 C_i}{\partial z^2} + \rho_B r_j, \quad (1)$$

$$\rho_g C_p v_Z \frac{\partial T}{\partial z} = \lambda_r \left(\frac{\partial^2 T}{\partial r^2} + \frac{1}{r} \frac{\partial T}{\partial r} \right) + \lambda_z \frac{\partial^2 T}{\partial z^2} + \rho_B \left[\sum -\Delta H_j r_j \right], \quad (2)$$

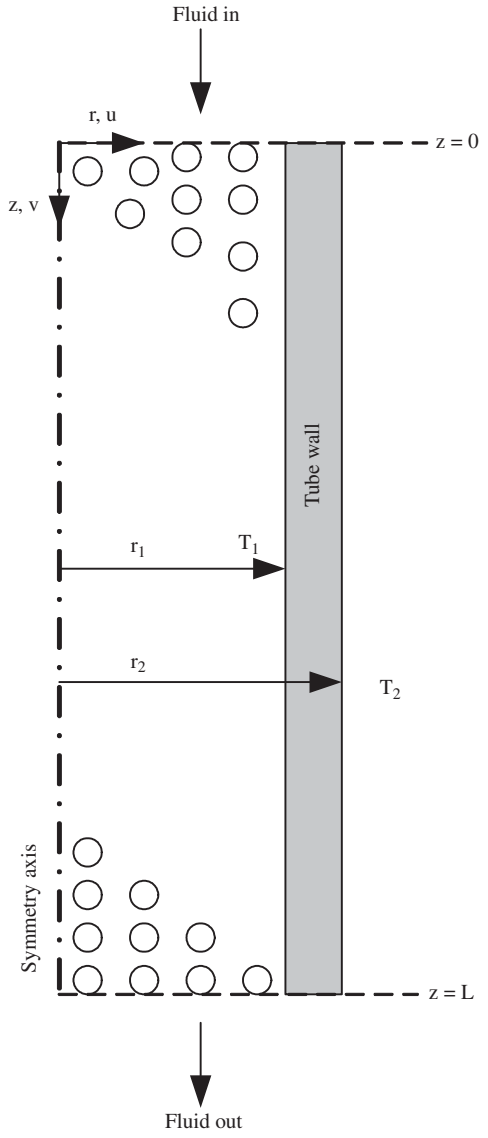

Fig. 1. A schematic diagram of the packed bed tubular reactor (PBTR).

where D_z and D_r, respectively, denote the effective diffusivity in axial and radial directions, λ_z and λ_r respectively, denote effective thermal conductivity in axial and radial directions, v denotes velocity, C_i denotes concentration of each chemical species, ρ_B denotes the catalyst bulk density, r_j denotes reaction rate (noting that if the diffusant is being consumed by the reaction, r_j is negative in these equations otherwise it is positive), ρ_g denotes gas density, C_p denotes heat capacity, T denotes temperature, and ΔH denotes heat of reaction.

The initial and boundary conditions for the steady state mass and energy balance equations (Eqs. (1) and (2)) in the case of using the PBTR shown in Fig. 1 are as follows:

$$C_i(r,0) = C_i^0, \quad T(r,0) = T^0 \quad \text{at } z = 0 \text{ and } 0 \leqslant r \leqslant r_1,$$

$$\frac{\partial C_i}{\partial r}(0,z) = 0, \quad \frac{\partial T}{\partial r}(0,z) = 0 \quad \text{at } r = 0 \text{ and } 0 \leqslant z \leqslant L,$$

$$\frac{\partial C_i}{\partial r}(r_1,z) = 0, \quad -\lambda_r \frac{\partial T}{\partial r}(r_1,z) = U_{TW}(T_1 - T_2) \quad \text{at } r = r_1 \text{ and } 0 \leqslant z \leqslant L,$$

where U_{TW} denotes overall heat transfer coefficient across the tube wall and the superscript 0 denotes the inlet conditions. Regarding the boundary conditions at the outlet of the reactor (at $z = L$ and $0 \leqslant r \leqslant r_1$), it can be assumed that the convective part of the mass and heat transport vector dominates. The finite element method was used to solve the partial differential equations (Eqs. (1) and (2)) subject to these initial and boundary conditions. It is important to note that these numerical model equations were solved without any simplifying assumptions such as eliminating the axial dispersion term or the cylindrical coordinates.

Before using this comprehensive model (Eqs. (1) and (2)) to simulate the production of hydrogen by the reforming of crude ethanol, it was essential to solve a well-documented problem as a validation of this model and the numerical techniques used to solve it. Froment and Bischoff [20] reported an industrial example for the partial oxidation of *o*-xylene in air to produce phthalic anhydride in a multi-tube fixed-bed reactor. In brief, the chemical reactions for the partial oxidation of *o*-xylene in air to phthalic anhydride can be presented as in Eq. (3):

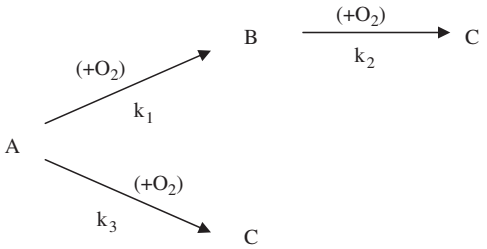

(3)

where A represents *o*-xylene, B represents phthalic anhydride, and C represents the total amount of carbon monoxide and carbon dioxide. Due to a very high excess of oxygen, the reactions can be considered to be pseudo-first-order, and the reactions kinetics can be described as in Eqs. (4)–(6) in terms of mole fraction:

$$r_A = y_A^0 y_{O_2}(k_1 + k_3)(y_A), \tag{4}$$

$$r_B = y_A^0 y_{O_2}[k_1 y_A - k_2 y_B], \tag{5}$$

$$r_C = y_A^0 y_{O_2}[k_2 y_B + k_3 y_A], \tag{6}$$

where y_{O_2} represents the mole fraction of oxygen, and y_A^0 is the inlet mole fraction of *o*-xylene. Furthermore, y_A is

the mole fraction *o*-xylene, y_B is the mole fraction of phthalic anhydride, and y_C represents the total mole fraction of carbon monoxide and carbon dioxide.

The rate coefficients, k_i, depend on temperature as described by the Arrhenius law according to the expressions in Eq. (7):

$$k_i = A_i \exp\left(\frac{-B_i}{T}\right), \tag{7}$$

where T is the temperature, and the constants A_i and B_i are as given in Table 1 for $i = 1, 2$, and 3.

The numerical model for this industrial scale example was also according to Eqs. (1) and (2), which was solved by finite element techniques subject to the initial and boundary conditions as well as the related modeling parameters presented in Table 1, column 5.

2.2. Kinetic model for production of hydrogen by reforming of crude ethanol

Before Eqs. (1) and (2) can be solved for the case of the production of hydrogen by the reforming of crude ethanol, it is essential to provide the kinetic model, r_j, that describes the reaction, j. The kinetic model for the production of hydrogen by reforming of crude ethanol that was used in conjunction with the numerical model (Eqs. (1) and (2)) was based on our earlier work documented elsewhere [19]. The model was obtained at temperatures in the range of 593–793 K, ratio of weight of catalyst to the mass flow rate of crude ethanol (W/F_{A0}) in the range 779–2143 kg-cat s/kg-crude ethanol. Based on earlier analysis as documented elsewhere [18,19], crude ethanol was defined on a volume basis as 12% ethanol, 1% lactic acid, 1% glycerol and 0.001% maltose, the balance being water. Also, the conversion of crude ethanol was as defined in Eq. (8). Based on these definitions, the kinetic model obtained is as shown in Eq. (9). Details of these analyses, generation of kinetic data as well as the derivation and validation of the kinetic model are reported elsewhere [19].

$$\text{Crude ethanol conversion } (X) = \frac{\text{gmol (organics)in} - \text{gmol (organics)out}}{\text{gmol(organics)in}}, \tag{8}$$

where organics = ethanol + lactic acid + glycerol + maltose

$$r_A = \frac{k_O e^{-E/RT}\left(N_A - N_C^2 N_D^6 / K_P N_B^3\right)}{[1 + K_A N_A]^2}. \tag{9}$$

It is important to note that H_2O was present in a large excess as compared to the concentration of the organic components of the crude, C_A, and also, the reaction was more or less irreversible within the temperature range used for the kinetic studies as shown by the values of thermodynamic equilibrium constant given in Table 1, which also contains all the values of the parameters in Eq. (9). The kinetics were based on the Eley Rideal mechanism.

3. Experimental work

3.1. Apparatus and procedures

Experimental kinetic data for H_2 production by the reforming of crude ethanol were obtained using a conventional catalytic PBTR operated isothermally at atmospheric pressure. The type of reactor used to obtain kinetic data was the BTRS Model, number 02250192-1 supplied by Autoclave Engineers. It was made of a stainless steel tube of 8 mm internal diameter placed concentrically in an electric furnace. Crude ethanol was supplied by means of high-pressure liquid chromatography (HPLC) pump regulated at the desired flow rates. The reaction temperature was measured with a sliding thermocouple placed inside the catalyst bed. The error on temperature measurement was within ±1 K.

A typical run for the reforming of crude ethanol was performed as follows: approximately 1 g of Ni/Al_2O_3 catalyst was mixed with 2 g of Pyrex glass (inert material) of the same average particle size and then loaded into the reactor. The feed consisting of crude ethanol (comprising of ethanol plus other organics and water) was then pumped at the desired flow rate (i.e. space velocity) to the vaporizer maintained at 523 K before entering the reactor. Prior to reaction, the catalyst was activated by in situ reduction with 5% H_2/N_2 gas (supplied by PRAXAIR, Regina, SK, Canada) flowing at 1.67×10^{-6} m^3/s for 2 h. The reactions were carried out at atmospheric pressure at temperatures in the range of 593–793 K. The product mixture during reaction was passed through a condenser and gas–liquid separator to separate the gaseous and liquid products for analysis.

3.2. Material analysis

The liquid product was analyzed using HPLC techniques as documented elsewhere [18]. The liquid product was also analyzed using a gas chromatograph–mass spectrometer (GC–MS) technique in order to identify the components for subsequent HPLC analysis and stoichiometric evaluations. GC–MS analysis was performed using GC–MS model HP 6890/5073 supplied by Hewlett-Packard Quebec, Canada. An HP-Innowax column (length = 30 m, internal diameter = 250 μm, thickness = 0.25 μm) packed with cross-linked-poly-ethylene glycol was used in the GC for the separation of components. The composition of the reformer product gas stream was analyzed on-line by gas chromatography (Model HP 6890) using molecular sieve and Haysep columns, and a thermal conductivity detector (TCD) with helium as the carrier gas.

3.3. Experimental data

The experiments to collect kinetic data were conducted over the catalyst bed in such a way that fluids channeling and back mixing were absent. These conditions were achieved by employing catalyst in the appropriate average size range,

Table 1
The operating conditions and parameters used in the numerical modeling of the laboratory tubular reactor and industrial scale multi-tubular reactor

Parameter	Definition and units	Crude ethanol lab scale[a]	Crude ethanol industrial[b]	*o*-xylene industrial case [20][c]
T_0	Feed inlet temperature, K	593	593	627
v_Z	Superficial velocity, m/s	—	1.0×10^{-3}	1.064×10^{-3}
W/F_{A0}	Space time, kg-cat s/kg-crude	2016	—	—
D_p	Catalyst particle diameter, mm	0.6	0.6	3
D_t	Internal diameter of the tube of the reactor, mm	8	24.5	25.4
R	Radius of packed bed tubular reactor, m	4×10^{-3}	12.7×10^{-3}	12.7×10^{-3}
L	Catalyst bed length, m	53×10^{-3}	3	3
ρ_g	Gas density, kg/m^3	0.31	0.31	1293
ρ_B	Bulk density of catalyst in the reactor, kg/m^3	375	1300	1300
λ_z and λ_r	Effective thermal conductivity, kJ/m s K	9.75×10^{-3}	9.75×10^{-3}	0.78×10^{-3}
C_p	Heat capacity, kJ/kg K	4.52	4.52	0.992
D_z and D_r	Effective diffusivity, m^2/s	3.2×10^{-7}	3.2×10^{-7}	3.19×10^{-7}
ΔH_1	Heat of reaction, kJ/kmol	3.056×10^5	3.056×10^5	-1.285×10^6
ΔH_3	Heat of reaction, kJ/kmol	—	—	-4.564×10^6
U_{TW}	Heat transfer coefficient, kJ/m^2 s K	0.156	0.156	0.156
k_0	Rate constant	2.08×10^3	2.08×10^3	—
E	Activation energy	4.43×10^3	4.43×10^3	—
K_A	Adsorption constant	3.83×10^7	3.83×10^7	—
P_{tot}	Total pressure, kPa	101.3	101.3	101.3
K_P	Equilibrium constant at T_0	2.454×10^{11}	2.454×10^{11}	
C_{tot}	Total concentration, kmol/m^3	—	—	44.85
C_A^0	Initial crude ethanol concentration, kmol/m^3	—	1.5	—
y_A^0	Inlet mole fraction of crude ethanol or *o*-xylene	0.054	0.054	0.00924
y_{O_2}	Inlet mole fraction of oxygen	—	—	0.208
M_{ave}	Average molecular weight of crude ethanol	51.29	51.29	—
A_1	Constant, Equation	—	—	1.145×10^5
A_2	Constant, Equation	—	—	3.185×10^5
A_3	Constant, Equation	—	—	4.811×10^5
B_1	Constant, Equation	—	—	13588
B_2	Constant, Equation	—	—	15803
B_3	Constant, Equation	—	—	14394

[a]Experimental data of crude ethanol reforming, run number CE01.
[b]Hypothetical industrial crude ethanol reformer.
[c]Partial oxidation of *o*-xylene, industrial data from reference number 20, section 11.5.2 and section 11.7.3.

appropriate feed space velocity and residence time as well as other conditions necessary and required for plug flow and isothermal behavior in the reactor. These conditions were experimentally determined using the procedure described by Idem and Bakhshi [27].

The experiments to collect kinetic data were eventually performed at reaction temperatures of 593, 693 and 793 K, and ratios of mass of catalyst to mass flow rate of crude ethanol (W/F_{A0}) of 779, 952, 1071, 1382, and 2143 kg-cat s/kg-crude ethanol using catalyst of 0.6 mm average particle size. According to Rase [28] and Froment and Bischoff [20], there are other criteria for packed-bed reactors to ensure that flow conditions in the reactor are close to plug flow in order to obtain isothermal reactor operation, eliminate backmixing and minimize channeling. These are: (a) ratio of catalyst bed height to catalyst particle size (L/D_p) > 50, and (b) ratio of internal diameter of the reactor to the catalyst particle size (D_t/D_p) > 10. In this work L/D_p and D_t/D_p of 88.33 and 13.33, respectively, were used in all kinetic experiments in an attempt to ensure plug flow behavior in the reactor.

4. Results and discussion

4.1. Model validation results

For the specific purpose of validating the numerical model and the method employed to solve it, we simulated a well-

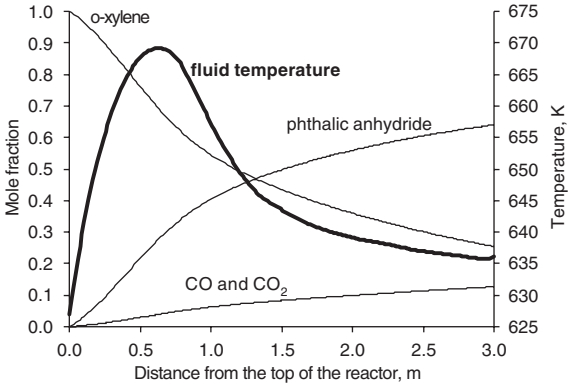

Fig. 2. Center line axial concentration and temperature profiles in multi-tubular *o*-xylene oxidation reactor (operating conditions and parameters are as presented in Table 3, column 5).

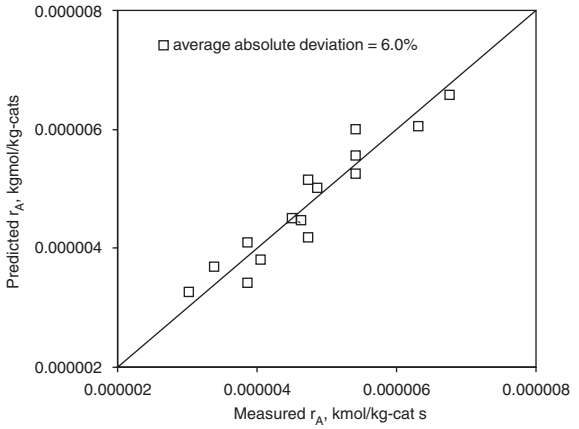

Fig. 3. Comparison of measured and predicted rates of reaction (mechanism based model of Eq. (9)) within the temperature range from 593 to 793 K and WHSV range from 4.67×10^{-4} to $1.28 \times 10^{-3}\ s^{-1}$.

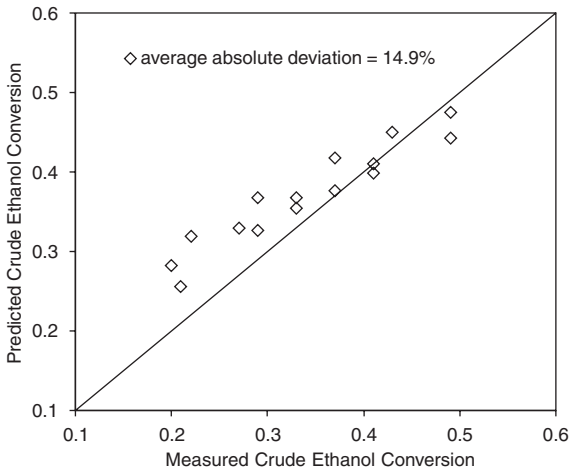

Fig. 4. Comparison of measured and predicted crude ethanol conversion within the temperature range from 593 to 793 K and WHSV range from 4.67×10^{-4} to $1.28 \times 10^{-3}\ s^{-1}$.

documented reaction process which involved the partial oxidation of *o*-xylene [20] using the model described in the present study. Although the simulation covered all aspects reported by Froment and Bischoff [20], only the axial concentration and temperature profiles are shown in the present work. The parameters used in the numerical modeling and simulation of the packed bed multi-tubular reactor for the partial oxidation of *o*-xylene are given in Table 1, column 5. Fig. 2 shows the axial concentration profiles obtained along the center of the reactor for an inlet temperature of 627 K for the partial oxidation of *o*-xylene. This figure shows results and behavior identical to those reported by Froment and Bischoff [20]. These results validate our formulation of the numerical model as well as the solution of the partial differential equations using finite element techniques without any simplifying assumptions.

Fig. 2 also shows the temperature profile along the tubular reactor as a further validation of our numerical model. A hot spot at the temperature of 669.2 K was reached close to the inlet at about 0.63 m from the top of the reactor. Again, this figure indicates results and behavior identical to those reported by Froment and Bischoff [20] for the temperature profile. According to these authors [20], the hot spot occurs at the identified location because of the exothermic nature of the chemical reaction combined with the fast rate of the reaction. In this case, cooling or catalyst dilution would be required to prevent a runaway temperature.

4.2. Kinetics data results

Experimental rates for the production of hydrogen by the reforming of crude ethanol were obtained and compared with those predicted by the rate model given in Eq. (9) for the mechanism based model. The results are shown in the parity chart shown in Fig. 3. This figure shows excellent predictive ability of the model with an average absolute deviations (AADs) of 6.0%. This shows that the assumptions made in terms of rate determining step for this Eley Rideal mechanism based model, Eq. (9) and neglecting the effects of the products for deriving the model were justified as documented elsewhere [19].

4.3. Numerical model predictive performance

The parameters used in the numerical modeling of the PBTR for the production of hydrogen by the reforming of crude ethanol are also presented in Table 1, columns 3 and 4. The simulation and experimental results are given in the parity chart of Fig. 4, which compares the experimental conversions of crude ethanol with those predicted by solv-

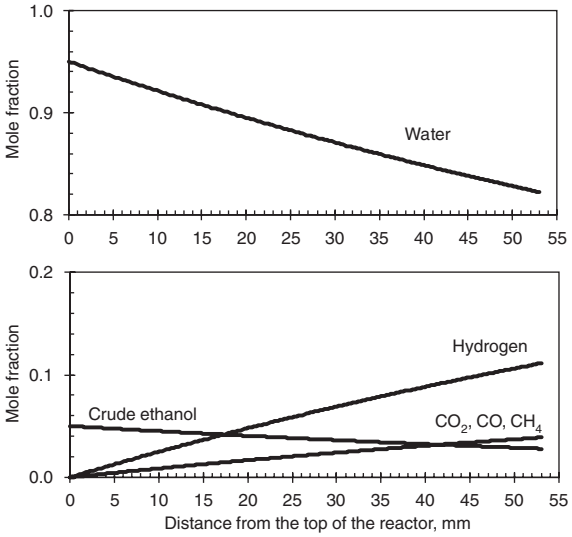

Fig. 5. Concentration profiles along the reactor at a feed temperature of 593 K and W/F_{A0} of 2016 kg-cat s/kg-crude.

ing the partial differential Eqs. (1) and (2) subject to the initial and boundary conditions and using the rate model given in Eq. (9). This figure shows very good predictive ability of the numerical model (Eqs. (1) and (2)) with an AAD from the experimental data of 15%. It is important to note that the numerical solutions were arrived at without any simplifying assumptions, unlike what is obtained in the literature [24], where the axial dispersion term is eliminated in order to simplify the solution of the partial differential equations. Our results show that conversions at the higher flow rates were slightly under-predicted by the model. We attributed this slight deviation to the fact that within this regime, slightly lower crude ethanol flow rates than those specified on the pump were obtained as a result of the back pressure developed within the reactor at the higher reaction temperatures for these flow rates as used for experiments. The consequence of this was that the real (i.e. slightly lower) experimental flow rates resulted in higher crude ethanol conversions within this regime, whereas the values specified on the pump were used for numerical modeling that resulted in the slightly lower conversions within this regime.

4.4. Simulation of concentration profiles of chemical species along the reactor length

The solution of the numerical model (i.e. the partial differential equations (1) and (2)) subject to the initial and boundary conditions in conjunction with the kinetic model (Eq. (9)) also enabled us to simulate the concentration profiles of all the species along the reactor. Typical profiles for crude ethanol feed temperature of 593 K and W/F_{A0} of 2016 kg-cat s/kg-crude ethanol is shown in Fig. 5. The exit concentrations based on the solution of the numerical model for the production of hydrogen from the reforming of crude ethanol for all the species for this run were compared with the corresponding concentrations obtained experimentally by GC and HPLC analyses. The results are given in Table 2. There is excellent agreement between the predicted and experimental results with an AAD% of 6.2%, indicating the power of the comprehensive numerical model used.

4.5. Effect of the axial dispersion term

As was mentioned earlier, most of the available reactor models often make simplifying assumptions [24,25]. We used our numerical model to determine the possible effects of neglecting axial dispersion as well as the conditions in which it is not appropriate to assume plug flow behavior. The simulated results in the case of neglecting or not neglecting axial dispersion are shown in Figs. 6 and 7 in terms of the radial conversion profile of crude ethanol and the radial temperature profile of the fluid in the reactor, respectively. The results exhibit more or less plug flow and isothermal behaviors. However, the results show that by neglecting the axial dispersion term, the crude ethanol conversion is under predicted (Fig. 6), and the extent of under prediction depends on the ratio of the velocity to the diffusivity (v_z/D_z) with a lower v_z/D_z ratio resulting in a lower prediction. Similar behavior and discussion is applied to the reaction temperature shown in Fig. 7. The slightly lower temperature shown in the center of the reactor is due to the endothermic nature of the reaction.

We tested isothermal and plug flow assumptions using a different set of conditions (outside the range used in obtaining kinetic data for this work). For example, we used an industrial reactor of internal diameter of 25.4 mm and 3 m length, and a smaller ratio of v_z/D_z equal to 3125 m^{-1}. The

Table 2
Outlet concentration profiles of the reactor at feed temperature of 593 K and W/F_{A0} of 2016 kg-cat s/kg-crude

Fluid	Measured mole fraction	Predicted mole fraction	AD%
Crude ethanol	0.029	0.028	3.45
Water	0.805	0.822	2.11
CO_2, CO, CH_4, etc.	0.043	0.039	9.30
Hydrogen	0.123	0.111	9.76
	Average absolute deviation, AAD%		6.15

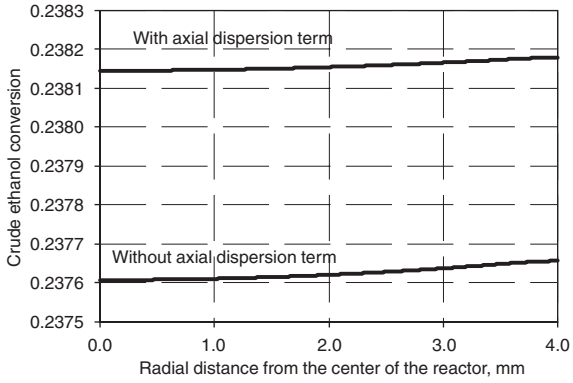

Fig. 6. Effect of axial dispersion term on the crude ethanol conversion profile at a depth of 30 mm from the top of the catalyst bed at a feed temperature of 593 K and W/F_{A0} of 2016 kg-cat s/kg-crude.

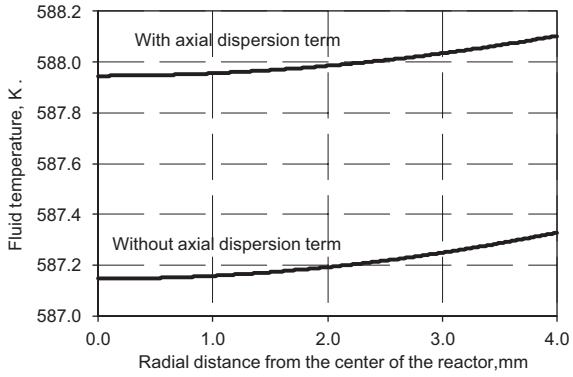

Fig. 7. Effect of axial dispersion term on the temperature profile at a depth of 30 mm from the top of the catalyst bed at a feed temperature of 593 K and W/F_{A0} of 2016 kg-cat s/kg-crude.

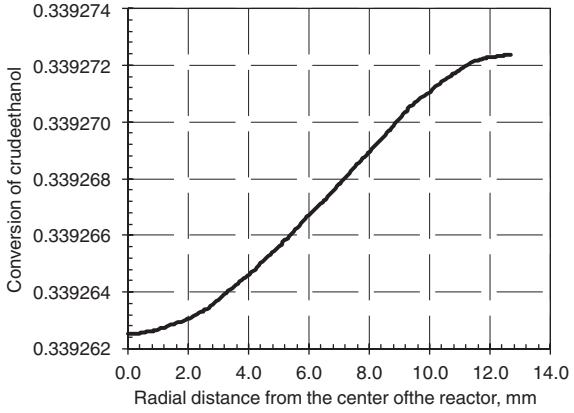

Fig. 8. Radial concentration profile of crude ethanol at a depth of 1.8 m from the top of the catalyst bed. The operating conditions and parameters used are presented in Table 1, column 4, for the hypothetical industrial crude ethanol reformer.

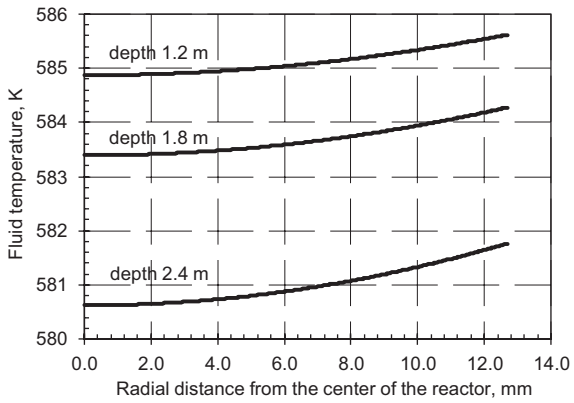

Fig. 9. Radial temperature profiles at various catalyst bed depths in the tubular reactor of the industrial crude ethanol reforming. The operating conditions and parameters used are presented in Table 3, column 4, for the hypothetical industrial crude ethanol reformer.

results are shown in Fig. 8 for the concentration profile of crude ethanol, and in Fig. 9 for the temperature profiles at different depths of the catalyst bed. These figures show that isothermal and plug behaviors were not attained. In addition, it can be seen from Fig. 9 that the radial temperature gradients are quite significant. An accurate determination of the heat flux, which is required for cooling or heating the reactor, can be obtained by solving the comprehensive model equations in both axial and radial directions without any simplification assumptions.

In brief, the above results, Figs. 6–9, show that the assumption of plug flow and isothermal behavior used in our work to obtain kinetic data was justified. They also show that since plug flow and isothermal behavior cannot always be guaranteed (even by following well-known criteria), it is very essential to use a comprehensive model to verify without simplifying assumptions whether or not plug flow and isothermal behavior are attained as well as whether the axial dispersion term significantly affects the model performance for the experimental conditions used.

4.6. Simulation of effect of reactor length and W/F_{A0}

In some instances, the objective of a process may be to enhance the performance of the reactor in a given process. Such an enhancement may be achieved by an increase in the length of the catalyst bed or and increase in W/F_{A0} ratio both of which result in an increase in the residence time of the feed in the reactor. We simulated the first effect with our experimental reactor for the production of hydrogen from the reforming of crude ethanol by increasing the catalyst bed length from 0.05 to 0.2 m at temperatures in the range of 373–873 K. The results are shown in Fig. 10 for a

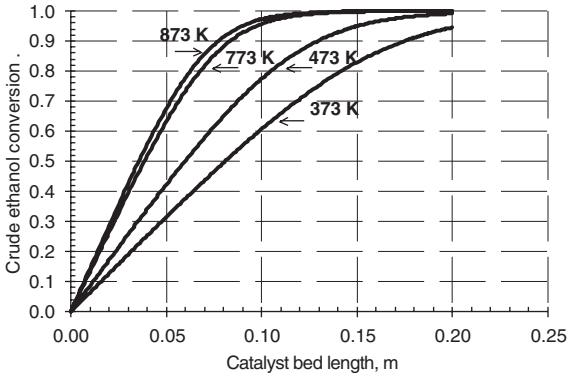

Fig. 10. Effect of catalyst bed length on crude ethanol conversion at various feed temperatures, catalyst bulk density of 1126 kg/m^3 and W/F_{A0} of 2000 s.

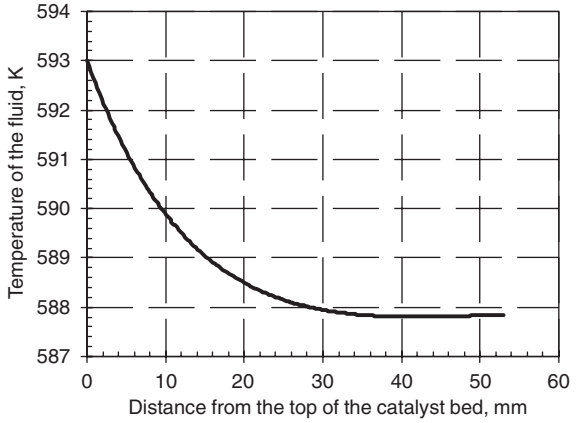

Fig. 11. Axial temperature profile of the fluid along the center of the tubular reactor at W/F_{A0} of 2016 kg-cat s/kg-crude and inlet feed temperature of 593 K. The parameters used are presented in Table 1, column 3.

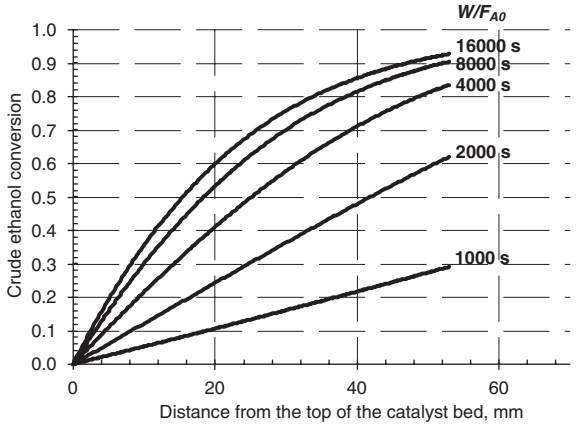

Fig. 12. Effect of W/F_{A0} on crude ethanol conversion in the axial direction at 693 K and bulk density of 1126 kg/m^3.

fixed W/F_{A0} ratio of 2000 s for this range of temperatures. These results show that even though there are some benefits to be derived by increasing the length of the catalyst bed, these benefits, however, diminish as the reaction temperature increases. In fact, at the highest temperatures used in this study, the benefit is so insignificant that the reaction is more or less completed after a catalyst bed length of about 0.15 m so that the extra length of catalyst bed beyond 0.15 m is not utilized. At the lower temperature (373 K), there is no additional conversion beyond 0.2 m. This is attributed to the higher degree of reversibility of the reaction at this temperature. Thus, irrespective of the temperature, the benefit of an increase in length is limited. The corresponding axial temperature profile for a run conducted at $W/F_{A0} = 2016$ kg-cat s/kg-crude and inlet feed temperature of 593 K is shown in Fig. 11. This figure shows a rapid drop in temperature at the top of the catalyst bed, which become slower after 20 mm depth as the feed progressed towards the bottom of the catalyst bed. This is a reflection of a slowing down of the reaction (crude ethanol conversion) as shown in Fig. 10, and consequently, a lesser endothermic demand for heat supply as the reaction mixture progresses towards the bottom of the catalyst bed.

In the case of a change in W/F_{A0} ratio, the results are given in Fig. 12 for a fixed catalyst bed length of 0.53 m and temperature of 693 K for W/F_{A0} in the range of 1000–16000 s. The results show that the benefit is huge (i.e. linear increase in the conversion of crude ethanol with W/F_{A0}) for the lower W/F_{A0} values. However, as the W/F_{A0} values increase (i.e. extremely low flow rates), the beneficial effects start to diminish. The effects of both the increase in catalyst bed length and the W/F_{A0} ratio on crude ethanol conversion demonstrate that there are limits as to how much enhancements could be achieved without modifying the activity of the catalyst to provide for higher activity. However, it points us to the region where we can maximize the gains by optimizing the relevant parameters for increasing the production of hydrogen by the reforming of crude ethanol.

5. Conclusions

A comprehensive model for the design and simulation of packed bed tubular reactors was developed for the catalytic reforming of crude ethanol to produce hydrogen. On both laboratory and industrial scales, the developed mathematical model is capable of accurately predicting the concentration profiles of all the chemical species and the temperature profiles of the fluid in both axial and radial directions. The simulation results on the laboratory scale as well as the industrial scale was able to demonstrate that plug flow and

isothermal behaviors could not always be guaranteed even by following well-known operating criteria. As a result, it is recommended to use a comprehensive model to verify whether or not plug flow behavior is attained for each kinetic experimental condition.

Acknowledgements

The financial support provided by the Canada Foundation for Innovation (CFI) and HTC Hydrogen Technologies Corporation, Regina, SK, Canada, is gratefully acknowledged.

References

[1] Creveling HF. Proton exchange membrane (PEM) fuel cell system R & D for transportation applications. In: Proceedings of the annual automotive technology development contractors' coordination meeting, Society of Automotive Engineers, October 19–21, 1992. p. 485–92.
[2] Dunnison DS, Wilson J. PEM fuel cells: a commercial reality. AIAA 29th intersociety energy conversion engineering conference, Monterey, CA, 1994. p. 1260–3.
[3] Whitaker FL. The phosphoric acid PC25^{TM} fuel cell power plant—and beyond. AIAA 29th intersociety energy conversion engineering conference, Monterey, CA, 1994. p. 1258–59.
[4] Gary JH, Handwerk GE. Petroleum refining technology and economics. 3rd ed., New York: Marcel Dekker; 1994.
[5] Simanzhenkov V, Idem RO. Crude oil chemistry. New York: Marcel Dekker; 2003.
[6] Garcia L, French R, Czernik S, Chornet E. Catalytic steam reforming of bio-oils for the production of hydrogen: effects of catalyst composition. Appl Catal 2000;201:225–39.
[7] Cortright RD, Davda RR, Dumesic JA. Hydrogen from catalytic reforming of biomass-derived hydrocarbon in liquid water. Lett Nat 2002;418:964–7.
[8] Haga F, Nakajima T, Yamashita K, Mishima S. Effect of crystallite size on the catalysis of alumina-supported cobalt catalyst for steam reforming of ethanol. React Kinet Catal Lett 1998;63(2):253–9.
[9] Cavallaro S, Freni S. Ethanol steam reforming in a molten carbonate fuel cell. A preliminary kinetic investigation. Int J Hydrogen Energy 1996;21(6):465–9.
[10] Athanasio NF, Verykios XE. Reaction network of steam reforming of ethanol over Ni-based catalysts. J Catal 2004;225:439–52.
[11] Athanasios NF, Kondaridesm DI. Production of hydrogen for fuel cells by reformation of biomass-derived ethanol. Catal Today 2002;75:145–55.
[12] Klouz V, Fierro V, Denton P, Katz H, Lisse JP, Bouvot-mauduit S, Mirodatos C. Ethanol reforming for hydrogen production in a hybrid electric vehicle: process optimization. J Power Source 2002;105:26–34.
[13] Jordi L, Ramirez P. Direct production of hydrogen from ethanol aqueous solutions over oxide catalysts. R Soc Chem Chem Commun 2001; 641–2.
[14] Leclerc S, Mann RF, Peppley BA. Evaluation of the catalytic ethanol-steam reforming process as a source of hydrogen-rich gas for fuel cells. The CANMET Energy Technology Centre (CETC), 1998.
[15] Galvita VV, Semin GL, Belyaev V, Semikolenov VA, Tsiakaras P, Sobyanin VA. Synthesis gas production by steam reforming of ethanol. Appl Catal A: General 2001;220:123–7.
[16] Das N. Low temperature steam reforming of ethanol. MSc thesis, Department of Chemical Engineering, University of Saskatchewan, Saskatoon, Canada, 2003.
[17] Idem R, Ibrahim HH, Tontiwachwuthikul P, Wilson M. Processing of non-purified ethanol from a glucose fermentation process for solid oxide fuel cell application. In: Gale J, Kaya Y, editors. Proceedings of the 6th international conference on greenhouse gas control technologies, Kyoto, Japan, October 1–4, 2002. Oxford, UK: Pergamon; 2003. p. 1825–8.
[18] Akande A, Idem R, Dalai A. Synthesis, characterisation and performance evaluation of Ni/Al_2O_3 catalysts for reforming of crude ethanol for hydrogen production. Appl Catal 2005;287:159–75.
[19] Akande A, Aboudheir A, Idem R, Dalai A. Kinetic modeling of hydrogen production by the catalytic reforming of crude ethanol over a co-precipitated Ni–Al_2O_3 catalyst in a packed bed tubular reactor. Int J Hydrogen Energy, December 2004, submitted for publication.
[20] Froment GF, Bischoff KB. Chemical reactor analysis and design. 2nd ed., New York: Wiley; 1990.
[21] Prabhu AK, Liu A, Lovell LG, Oyama ST. Modeling of the methane reforming reaction in hydrogen selective membrane reactors. J Membr Sci 2000;177:83–95.
[22] Basile A, Paturzo L, Lagana F. The partial oxidation of methane to syngas in a palladium membrane reactor: simulation and experimental studies. Catal Today 2001;67: 65–75.
[23] Gallucci F, Paturzo L, Basile A. A simulation study of the steam reforming of methane in a dense tubular membrane reactor. Int J Hydrogen Energy 2004;29:611–7.
[24] Assabumrungrat S, Rienchalanusarn T, Praserthdam P, Goto S. Theoretical study of the application of porous membrane reactor to oxidative dehydrogenation of *n*-butane. Chem Eng J 2002;85:69–79.
[25] Basile A, Paturzo L, Vazzana A. Membrane reactor for the production of hydrogen and higher hydrocarbons from methane over Ru/Al_2O_3 catalyst. Chem Eng J 2003;93:31–9.
[26] Bird RB, Stewart WE, Lightfoot EN. Transport phenomena. 2nd ed., New York: Wiley; 2002.
[27] Idem RO, Bakhshi NN. Kinetics modeling of the production of hydrogen from methanol-steam reforming process over Mn-promoted coprecipitated Cu–Al catalyst. Chem Eng Sci 1996;51(14):3697–708.
[28] Rase HF. Chemical reactor design for process plants. New York: Wiley; 1987, 185–8, 195–259.